The Height of Biomolecules Measured with the Atomic Force Microscope Depends on Electrostatic Interactions

Daniel J. Müller*# and Andreas Engel*
*M. E. Müller Institute for Microscopic Structural Biology, Biozentrum, University of Basel, CH-4056 Basel, Switzerland, and #Forschungszentrum Jülich, Structural Biology, D-52425 Jülich, Germany

ABSTRACT In biological applications of atomic force microscopy, the different surface properties of the biological sample and its support become apparent. Observed height differences between the biomolecule and its supporting surface are thus not only of structural origin, but also depend on the different sample-tip and support-tip interactions. This can result in negative or positive contributions to the measured height, effects that are described by the DLVO (Derjaguin, Landau, Verwey, Overbeek) theory. Experimental verification shows that the electrostatic interactions between tip and sample can strongly influence the result obtained. To overcome this problem, pH and electrolyte concentration of the buffer solution have to be adjusted to screen out electrostatic forces. Under these conditions, the tip comes into direct contact with the surface of support and biological system, even when low forces required to prevent sample deformation are applied. In this case, the measured height can be related to the thickness of the native biological structure. The observed height dependence of the macromolecules on electrolyte concentration makes it possible to estimate surface charge densities.

INTRODUCTION

Because the atomic force microscope (AFM) (Binnig et al., 1986)) makes it possible to image surfaces in liquids, it has become an important tool for studying biological samples (Drake et al., 1989). Recent reports document the observation of protein assemblies under physiological conditions at nanometer resolution (Butt et al., 1990; Hoh et al., 1991; Karrasch et al., 1993, 1994; Yang et al., 1993; Schabert and Engel, 1994; Mou et al., 1995b; Müller et al., 1995b, 1996b). As demonstrated on solids under vacuum conditions (Sugawara et al., 1995) and in liquid (Ohnesorge and Binnig, 1993), the AFM also makes it possible to measure sample heights with subangstrom accuracy. However, the heights of native biological samples measured with the AFM in aqueous solution vary significantly, and may differ from values estimated with other methods (Butt et al., 1991; Apell et al., 1993; Müller et al., 1995b, 1996a; Schabert and Rabe, 1996). For example, the height reported for single purple membranes ranges from 5.1 ± 0.1 nm to 11.0 ± 3.4 nm (see Table 1). Height measurements on actin filaments (Fritz et al., 1995b), bacteriophage ø29 connectors (Müller et al., 1997c), cholera toxin (Yang et al., 1994; Mou et al., 1995b), DNA (Hansma et al., 1995; Mou et al., 1995a; Wyman et al., 1995), gap junctions (Hoh et al., 1993), GroEL (Mou et al., 1996), hexagonally packed intermediate layer (HPI) (Karrasch et al., 1993; Müller et al., 1996a; Schabert and Rabe, 1996), lipid bilayers (Mou et al., 1994, 1995b; Rädler et al., 1994), and microtubules (Fritz et al., 1995a) exhibit a similar variability. Height anomalies of soft surfaces have previously been studied and attributed to the mechanical properties of the sample (Weisenhorn et al., 1992; Radmacher et al., 1993, 1995; Hoh and Schoenenberger, 1994). However, thin samples such as two-dimensional protein arrays or biological membranes adsorbed to a solid support are not sufficiently compressible to explain such large height variation.

Here we demonstrate that electrostatic interactions between the AFM tip and the sample (Butt, 1991a,b) influence the measured height of a biological structure adsorbed to a solid support in buffer solution. The DLVO (Derjaguin, Landau, Verwey, Overbeek) theory (Israelachvili, 1991) is used to describe the electrostatic repulsion and van der Waals attraction acting between tip and sample (Butt et al., 1995). Experimental results and calculations show that the electrostatic double-layer forces can be eliminated by adjusting the electrolyte concentration (Butt, 1992a,b), providing conditions for correct height measurements with the AFM. In addition, the observed height dependence of the biological structure on electrolyte concentration allows its surface charge density to be estimated.

MATERIALS AND METHODS

Biological samples

Aquaporin-1 (AQP1) from human erythrocyte solubilized in octyl-β-glucopyranoside was reconstituted in the presence of *Escherichia coli* phospholipids to form two-dimensional (2D) crystalline sheets (Walz et al., 1994). The 2D crystals were prepared at a concentration of ~0.5 mg protein/ml and 0.25 mg/ml lipid in 0.25 M NaCl, 20 mM $MgCl_2$, 20 mM 2-(*N*-morpholino)ethanesulfonic acid (MES) (pH 6).

Hexagonally packed intermediate (HPI) layer from *Deinococcus radiodurans*, a kind gift of Dr. W. Baumeister, was extracted from whole cells (strain SARK) with lithium dodecyl sulfate, and purified on a Percoll density gradient (Baumeister et al., 1982). A stock solution (1 mg/ml protein) was stored in distilled water at 4°C.

Purple membranes of *Halobacterium salinarium* strain ET1001 were isolated as described by Oesterhelt and Stoeckenius (1974). The mem-

Received for publication 3 February 1997 and in final form 16 May 1997.
Address reprint requests to Dr. Andreas Engel, M. E. Müller Institute, Biozentrum, University of Basel, Klingelbergstrasse 70, CH-4056 Basel, Switzerland. Tel.: 0041-61-267-22-61; Fax: 0041-61-267-22-59; E-mail: aengel@ubaclu.unibas.ch.

0006-3495/97/09/1633/12 $2.00

TABLE 1 Different heights of purple membrane

Height	Support	Conditions	Method	Reference
8.9 ± 2 nm	Mica	2 mM $CaCl_2$, 80 mM KCl or NaCl, pH ranging from 4.0–6.5	AFM, contact	(Butt et al., 1990)
11.1 ± 3.4 nm	Silanized glass	1 mM $CaCl_2$, 10 mM KCl, 10 mM Tris, pH 7.2	AFM, contact	(Butt et al., 1990)
5.2 ± 0.2 nm	Lipid bilayer (DMPC)	Distilled water	AFM, contact	(Butt et al., 1990)
5.6 ± 0.1 nm	Mica	150 mM KCl, 10 mM Tris, pH ≥ 6.0	AFM, contact	(Müller et al., 1995b)
5.1 ± 0.1 nm	Mica	150 mM KCl, 10 mM Tris, pH ≤ 4.0	AFM, contact	(Müller et al., 1995b)
6.3 ± 0.4 nm	Mica	10 mM Tris, pH 8.2	AFM, contact	(Schabert and Rabe, 1996)
4.9 ± 1 nm	Carbon film	Embedded in glucose	Electron crystallography	(Henderson et al., 1990)
Lamellar spacing 5.3 nm (1) and 4.9 nm (2)	Stacks of membrane	Dried after adsorption at pH 10.0 (1) and pH 4.0 (2)	X-ray scattering	(Henderson, 1975)

branes were frozen and stored at −70°C. After thawing, stock solutions (10 mg protein/ml) were kept in distilled water at 4°C.

Porin OmpF trimers from *E. coli* strain BZ1110/PMY222 (Hoenger et al., 1993) solubilized in octyl-polyoxyethylene were mixed with solubilized dimyristoyl phosphatidylcholine (99% purity; Sigma Chemical Co., St. Louis, MO) at a lipid-to-protein ratio (w/w) of 0.2 and a protein concentration of 1 mg/ml. The mixture was reconstituted as previously described (Hoenger et al., 1993) in a temperature-controlled dialysis device (Jap et al., 1992). The dialysis buffer was 20 mM HEPES, pH 7.4, 100 mM NaCl, 20 mM $MgCl_2$, 0.2 mM dithiothreitol, 3 mM azide.

1,2-Dipalmitoyl-phosphatidylethanolamine (DPPE) from Sigma was solubilized in chloroform:hexane (1:1) to a concentration of 1 mg/ml. The resulting solution was diluted in buffer solution (150 mM KCl, 10 mM Tris, pH 8.4) to a concentration of 100 μg/ml.

Layered crystals

$MoTe_2$, a layered crystal of the family of transition metal dichalcogenides (Wilson and Yoffe, 1969), was employed to calibrate the piezo scanner of the AFM. It was prepared by chemical vapor transport (CVT), with chlorine or bromine as carrier gases in a temperature gradient of 100°C across the quartz ampule (Jungblut et al., 1992), and was a kind gift of Y. Tomm.

Muscovite mica (Mica New York Corp., New York) was used as the solid support for all samples. Mica minerals are characterized by their layered crystal structure, and show a perfect basal cleavage that provides atomically flat surfaces over several hundreds of square microns. Their hydrophilicity and relative chemical inertness (Bailey, 1984) make them suitable for the adsorption of biological macromolecules.

Atomic force microscopy

A commercial AFM (Nanoscope III; Digital Instruments, Santa Barbara, CA), equipped with a 120-μm scanner (j-scanner) and a liquid cell, was used. Before use, the liquid cell was cleaned with normal dish cleaner, gently rinsed with ultrapure water, sonicated in ethanol (50 kHz), and sonicated in ultrapure water (50 kHz). Mica was punched to a diameter of ~5 mm and glued with water-insoluble epoxy glue (Araldit; Ciba Geigy AG, Basel, Switzerland) onto a Teflon disc. Its diameter of 25 mm was slightly larger than the diameter of the supporting steel disc. The steel disc was required to magnetically mount the sample on to the piezoelectric scanner. Imaging was performed in the error signal mode, acquiring the deflection and height signal simultaneously. The deflection signal was minimized by optimizing gains and scan speed. The height images presented were recorded in the contact mode. The scan speed was roughly linear to the scan size, at 4–8 lines/s for lower magnifications (frame size 1–25 μm). The applied force was corrected manually to compensate for thermal drift. To achieve reproducible forces, cantilevers were selected from a restricted area of one wafer. The dimensions of one tip were measured in a scanning electron microscope to calculate the mechanical properties of the cantilever (Butt et al., 1993). The 120-μm-long cantilevers purchased from Olympus Ltd. (Tokyo, Japan) had a force constant of k = 0.1 N/m, and the 200-μm-long cantilevers purchased from Digital Instruments had a force constant of 0.15 N/m. All cantilevers used had oxide-sharpened Si_3N_4 tips.

Sample preparation

To minimize contamination of surfaces during exposure to ambient air, sample supports were prepared immediately before use. All buffers were made with ultrapure water (~18 $M\Omega cm^{-1}$; Branstead, Boston, MA). This water contains fewer hydrocarbons than conventional bidistilled water and fewer macroscopic contaminants, both of which can influence the imaging process. Chemicals were grade p.a. and purchased from Sigma Chemie AG (Buchs, Switzerland). The buffers used were Tris-(hydroxymethyl)-aminomethane (from pH 10.2 to pH 7.2), MES (from pH 6.5 to pH 5.5), and citric acid (from pH 5.4 to pH 3.0). Macromolecular samples were checked before use by conventional negative stain electron microscopy (Bremer et al., 1992) and/or by sodium dodecyl sulfate-gel electrophoresis.

The samples were diluted to a concentration of 5–10 μg/ml in buffer solution (pH 8.2, 20 mM Tris-HCl, ≥100 mM; monovalent electrolyte; except for DPPE, which was not further diluted) before adsorption to freshly cleaved mica. After an adsorption time of 10–60 min, the samples were gently washed with the measuring buffer to remove weakly attached membranes. This allowed height measurements at low electrolyte concentrations, at which samples adsorb sparsely to mica (Müller et al., 1997a and 1997b). Experiments requiring constant pH were performed at pH 8.2. The isoelectric points of bacteriorhodopsin, AQP1, DPPE, and OmpF are 5.2 (Ross et al., 1989), 6.95 (calculated), ~10 (Tatulian, 1993), and 4.64 (calculated), respectively. Thus, at this pH, all samples had a net negative charge, except for DPPE, which had a net positive charge.

RESULTS

Height calibration

Fig. 1 *a* shows a height image of the cleavage plane of $MoTe_2$ recorded in electrolyte solution (100 mM KCl). $MoTe_2$ consists of trigonal prismatic elements held together

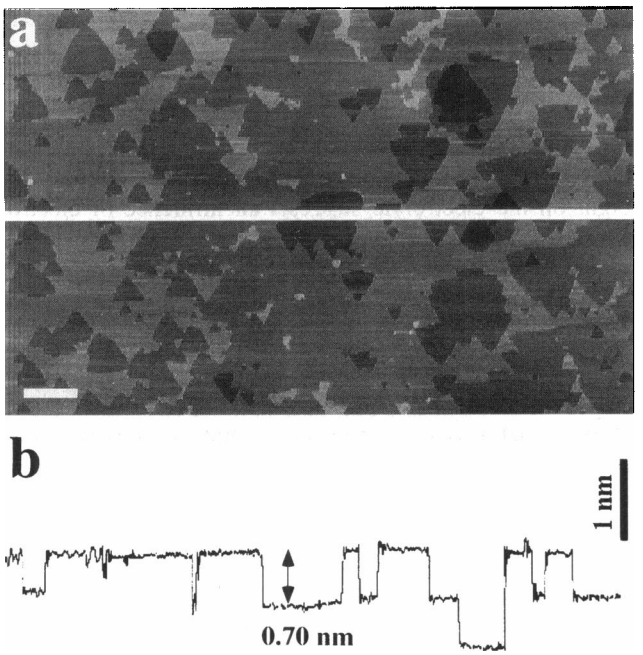

FIGURE 1 Vertical calibration of the piezo scanner using defects of the layered crystal $MoTe_2$. (*a*) Height image of the etched surface (scale bar = 500 nm). The crystal layers are visible, and the triangular defects can be directly related to the trigonal prismatic elements that assemble the layers. (*b*) Height profile along the line indicated in *a*. The height differences were multiples of a single crystal layer thickness including the van der Waals gap (c = 0.698 nm).

by covalent bonds within the layer (Wilson and Yoffe, 1969). Adjacent layers are held together by van der Waals forces. Cleavage with scotch tape provides atomically flat surfaces over several hundred square microns. In electrolyte solution, the layers are etched along the crystal plane of the trigonal prismatic elements. The resulting defects represent multiples of the thickness of the single crystal layer (0.698 nm), including the van der Waals gap between the layers (Fig. 1 *b*).

Electrolyte- and force-dependent heights measured on purple membranes

Fig. 2 *a* shows a representative topograph of purple membrane adsorbed to freshly cleaved mica in buffer solution (100 mM NaCl, 20 mM Tris-HCl, pH 8.2). A ring of lipid bilayer from the inner membrane of *Halobacterium salinarium* surrounded the bacteriorhodopsin lattices. The membranes had diameters of up to 1 μm, and the clean background of the image demonstrated that there were no other macromolecules adsorbed to the supporting surface or to the purple membrane sheet. This was a prerequisite for the high-resolution imaging required to identify the side of the membrane exposed to the tip (Fig. 2 *a*, *inset*; Müller et al., 1996b). Contaminants may also influence the overall height measured. The line used to determine the height between purple membrane and mica is indicated in Fig. 2 *a*. When forces of ~0.1 nN were applied to the tip during imaging, the purple membrane showed a height of 8.2 ± 0.4 nm (Fig. 2 *b*, *top*). When imaged at forces of ~1 nN, it exhibited a height of 5.5 ± 0.4 nm (Fig. 2 *b*, *bottom*).

To gain insight into this force dependence, force curves were recorded on purple membrane (Fig. 2 *c*; *solid line*) and on mica (Fig. 2 *c*; *dotted line*) directly after the image shown in Fig. 2 *a* was taken. To this end, the cantilever was pushed toward the sample (from right to left in the plot shown in Fig. 2 *c*), and its deflection was simultaneously monitored. The deflection was plotted along the vertical axis, taking the force calibration calculated from the geometry of the cantilever (see Materials and Methods). Differences between

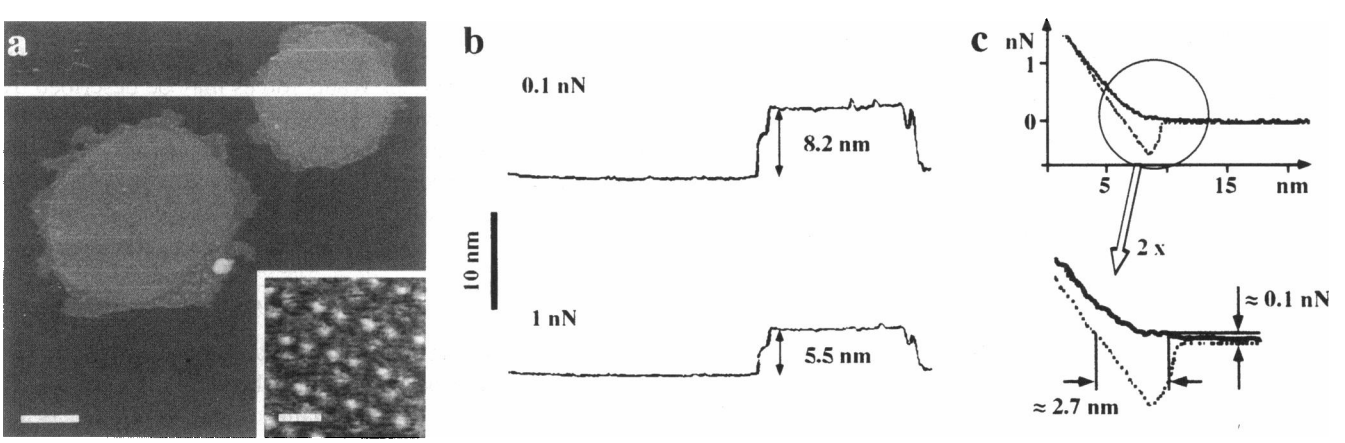

FIGURE 2 Purple membrane in buffer solution (100 mM NaCl, 20 mM Tris-HCl, pH 8.0). (*a*) The height image shows bacteriorhodopsin sheets surrounded by the lipid bilayer from the inner membrane of *Halobacterium salinarium*. The white line indicates the height line in *b*, and the inset displays the extracellular purple membrane surface at high resolution. The height between the protein layer and the mica surface (*b*) was determined to be 5.5 ± 0.4 nm (n = 50) at a force of 1 nN, but was 8.2 ± 0.4 nm (n = 64) when the force was 0.1 nN. (*c*) Force curves recorded on purple membrane (——) and mica (·····). Each force curve represents an average of 10 measurements, scan frequency 1.97 Hz, scan range 50 nm (512 pixels). The differences in the 0.1-nN range are clearly visible in the enlargement. Imaging conditions: ~0.3 nN and 0.2 nN for high resolution (*inset*), scan frequency 4.7 Hz. Scale bars are 200 nm and 5 nm in *a* and in the inset, respectively. The gray scales from dark to light shades represent 20 nm in *a* and 0.5 nm in the inset.

the two force curves larger than 0.5 nm only occurred at forces below 0.5 nN. In this region, the force curve on purple membrane showed a small repulsive interaction, which prevented the tip from coming into contact with the membrane surface. In contrast, the force curves recorded on mica showed no repulsive interaction, but rather a significant attraction revealed by the "jump in," promoting contact between tip and mica. The vertical difference between the tip-mica and the tip-membrane separations was ~2.7 ± 0.5 nm at forces of 0.1 nN (Fig. 2 *c*). The height measured at this force, 8.2 nm, was thus a composite of the thickness of purple membrane (~5.5 nm) and of the repulsive contribution Δz (2.7 nm). The lipid annulus exhibited similar force-dependent behavior. Its thickness was 5.5 ± 0.3 nm at low force (Fig. 2 *b*, *top trace*), and 3.2 ± 0.3 nm at high force (Fig. 2 *b*; *lower trace*).

Fig. 3 shows the dependence of measured purple membrane heights on electrolyte type and concentration. The force applied to the tip was kept between 0.1 and 0.2 nN throughout the experiments. Although all values were recorded at pH 8.0 ± 0.2, the height for a single membrane layer varied from 12.1 ± 1.2 nm (n = 45) to 5.5 ± 0.4 nm (n = 58). The smallest values were recorded at the highest salt concentrations, the largest values at the lowest salt concentrations. The orientation of each membrane patch with respect to the support was determined from its morphology observed at high magnification (Fig. 2 *a*, *inset*). No correlation between the orientation and the heights was detected. The clear dependence of the measured sample height on the electrolyte suggests an influence of electrostatic forces.

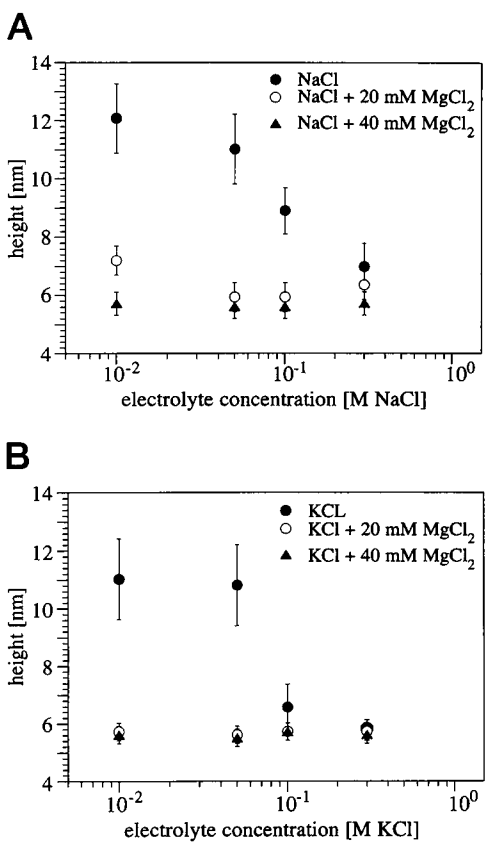

FIGURE 3 Height of purple membrane sheets supported on mica as a function of the electrolyte and its concentration. Each point represents an average of more than 40 measurements on different membranes. The constant force applied during measurements was between 0.1 and 0.2 nN. The solutions were buffered by 1–20 mM Tris (pH 8.2).

Electrostatic forces

Biological macromolecules and most of the supports used for atomic force microscopy (e.g., mica, graphite, Si, glass) exhibit a net surface charge in an aqueous environment, because acidic and basic functional groups at their surface dissociate according to their pK values. The magnitude and sign of the surface charge therefore depend on the pH of the buffer solution. The net surface charge is compensated by counterions from the bulk solution. The Debye length λ_D characterizes the exponential decrease in the potential resulting from screening the surface charges with electrolytes. λ_D can also be understood as the thickness of the diffuse electrical double layer formed by the counterions. As shown in Eq. 1, λ_D depends upon the valence and the concentration e_c of the electrolyte present (Israelachvili, 1991):

$$\lambda_D = \frac{0.304}{\sqrt{e_c}}\ \text{nm} \quad \text{for monovalent electrolytes}$$

$$= \frac{0.174}{\sqrt{e_c}}\ \text{nm} \quad \text{for divalent (1:2 or 2:1) electrolytes}$$

$$= \frac{0.152}{\sqrt{e_c}}\ \text{nm} \quad \text{for divalent (2:2) electrolytes} \qquad (1)$$

When the electrical double layers of two approaching surfaces overlap, an electrostatic interaction arises. This occurs at separations of a few tens of nanometers, where the van der Waals forces also play a role. The interplay between electrostatic and van der Waals forces may be described by the DLVO theory, neglecting effects of ion radii, hydration forces, steric forces, and specific interactions. The total force F_{DLVO}, between a sphere of radius R interacting with a planar surface is given by (Israelachvili, 1991)

$$F_{DLVO}(z) = F_{el}(z) + F_{vdW}(z) = \frac{4\pi\sigma_s\sigma_t R\lambda_D}{\epsilon_e\epsilon_0} e^{-z/\lambda_D} - \frac{H_a R}{6z^2} \qquad (2)$$

where σ_s and σ_t are the surface charge densities of sample and tip, ϵ_0 is the permittivity of the free space, ϵ_e is the dielectric constant, H_a is the Hamaker constant, and z is the distance between the two surfaces.

The surface properties of both the AFM tip and the sample define the electrostatic double-layer interaction (surface charge density) and the van der Waals attraction (Hamaker constant). The surface charge densities for Si_3N_4 (tip), mica (support), and purple membrane in water (around pH 7.0) are about −0.032 C/m^2 (Butt, 1991b), −0.0025

C/m^2 (Pashley, 1981), and -0.05 C/m^2 (Butt, 1992a), respectively. The Hamaker constants for hydrocarbons, mica, and metals in water are ~ 0.2–1×10^{-20} J (Butt et al., 1995), 2×10^{-20} J (Israelachvili, 1991, 1994), and 30–50×10^{-20} J (Israelachvili, 1991), respectively. Whereas the van der Waals force, F_{vdW}, is mainly unaffected by the electrolyte concentration and pH of the buffer solution, the electrostatic force, F_{el}, depends on these variables. This allows the distance-dependent interaction between tip and object to be tuned via the electrolyte to be attractive, repulsive, or repulsive and attractive, as discussed previously (Butt, 1991a,b, 1992a,b; Ducker et al., 1991). Once the tip comes into contact with the sample, the respective electron orbitals overlap, resulting in the very short-range, strong Pauli repulsion.

The electrolyte effect recorded by the force curves (Butt, 1991a,b, 1992a,b) must be considered when the AFM is operated in the constant force mode. In this mode, if the sample consists of two materials with different surface charge densities, the distance z of the tip from each of the surfaces will also be different (see Eq. 2). Thus the measured height h exhibits structural information, expressed as d, and information about the material properties of the tip and the biological sample, expressed as Δz (see Fig. 4). To evaluate Δz as a function of the salt concentration, the total force acting between a spherical Si_3N_4 tip and mica (Fig. 5 *a*), and a spherical Si_3N_4 tip and purple membrane (Fig. 5 *b*), was calculated according to Eq. 2. For simplicity, possible differences in the Hamaker constant describing the van der Waals interaction between Si_3N_4 tip and mica, and between the tip and purple membrane for the various electrolytes were neglected. Because the Hamaker constant of hydrocarbons immersed in water is ~ 0.2–1×10^{-20}J (Butt et al., 1995) and that of mica is 2×10^{-20} J (Israelachvili, 1991), a value of 1×10^{-20} J was assumed. As illustrated by Fig. 5, the electrostatic repulsion decreases with increasing electrolyte concentration. At sufficiently high electrolyte concentrations and very small separations (~ 2 nm), the van der Waals attraction becomes predominant. Because the surface charge density of purple membrane is 20 times larger than that of mica, screening of the electrostatic repulsion requires higher salt concentrations than for mica.

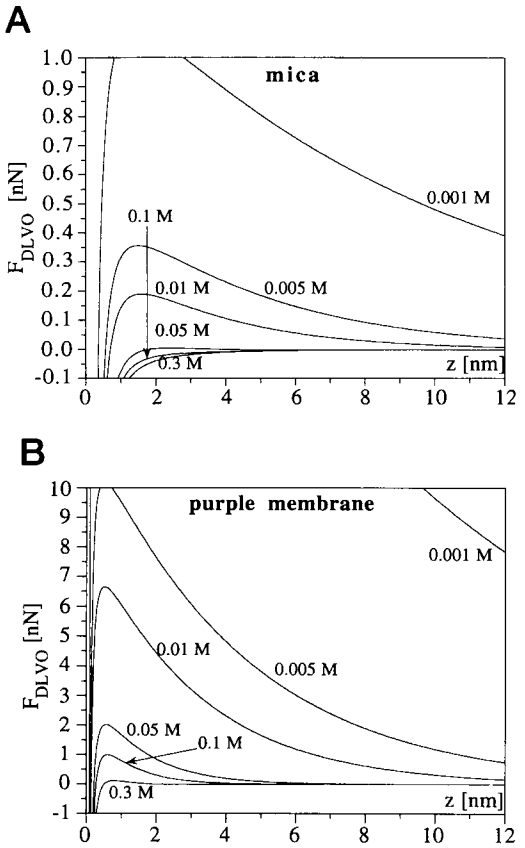

FIGURE 5 Calculated repulsive force between Si_3N_4 tip and mica (*a*) and between Si_3N_4 tip and purple membrane (*b*) at distance z from the surface in an aqueous monovalent electrolyte solution (pH 7.0). With increasing electrolyte concentration, the double-layer repulsion is progressively screened until the attractive van der Waals force is stronger. The surface charge density of purple membrane is ~ 20 times larger than that of mica. Consequently, the electrostatic interaction is stronger, and compared to mica, higher salt concentrations are needed to screen the repulsive force. Conditions: tip radius 100 nm, surface charge densities as cited in the text.

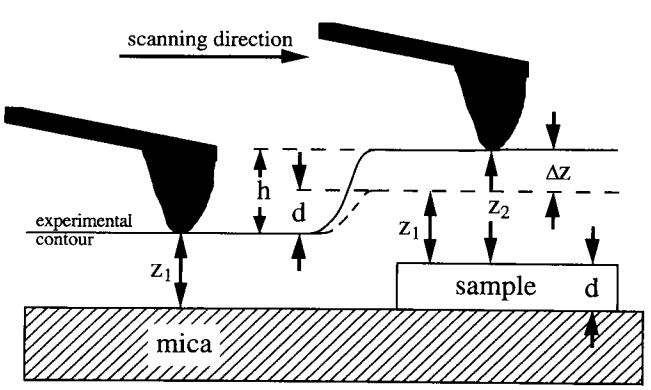

FIGURE 4 Schematic of the electrostatic height contribution measured with the AFM operated in the constant force mode in solution. The surface charge densities σ of support ($\sigma_{support}$) and object (σ_{object}) are assumed to be different. Consequently, at constant force the distance between tip and support, z_1, and between tip and object, z_2, must also be different ($\Delta z \neq 0$). Because the measured height h, is a composite of the structural height d and the difference of the tip-sample distances Δz, a systematic error occurs on height measurement, $h = d + \Delta z$.

In Fig. 6 the calculated height of purple membrane is plotted as a function of the force, which can be directly related to the force applied to the AFM tip. The structural height of purple membrane ($d \approx 5.6$ nm at pH 7.0; Müller et al., 1995b) and the difference Δz between the vertical tip-mica and tip-purple membrane distances for a given force and monovalent electrolyte concentration were employed (see Figs. 4 and 5). The measured heights depend on the force applied to the tip, as long as an electrostatic repulsion exists. Once the electrostatic repulsion is screened by the electrolyte for both support and sample, the height measured is the actual thickness of the purple membrane layer, and as such, in the absence of deformation, is inde-

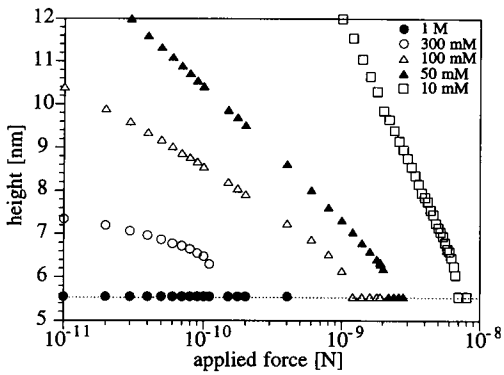

FIGURE 6 Force-dependent height of purple membrane adsorbed on mica and imaged with a Si_3N_4 tip of 100 nm radius. The values represent the differences in the vertical distances between tip and mica, and tip and purple membrane, as calculated in Fig. 5. The thickness of the purple membrane was assumed to be 5.6 nm as measured at pH 7.0 (·····; Müller et al., 1995b).

pendent of the applied force pushing the tip toward the sample surface.

A direct verification of the calculated force dependence on the electrolyte concentration is provided by the experimental force curves shown in Fig. 7, which were acquired on purple membrane (*solid lines*) and on mica (*dotted lines*). Each graph was recorded directly after the membranes had been imaged in the respective electrolyte. At low monovalent electrolyte concentrations (≤50 mM), the force curves showed repulsive forces for both purple membrane and mica. There was a long-range repulsive interaction that increased slowly at low forces. This explains the large standard deviation of purple membrane heights detected under such conditions (Fig. 3). The repulsive interaction decreased with increasing electrolyte concentration. Accordingly, the standard deviation of the height measurements also decreased (cf. Fig. 3). Divalent ions had a more pronounced effect in decreasing the double-layer thickness than monovalent ions. As explained by their smaller Debye length, divalent ions reduce the double layer thickness more quickly by a factor of ~2 (Israelachvili, 1991; see also Eqs. 1 and 2).

The heights of other planar biological structures

Fig. 8 *a* shows DPPE bilayers in a weakly buffered aqueous 5 mM KCl solution at pH 8.2. The bilayers were adsorbed to freshly cleaved mica as described in Müller et al., 1997a. They formed continuous layers surrounding defects of var-

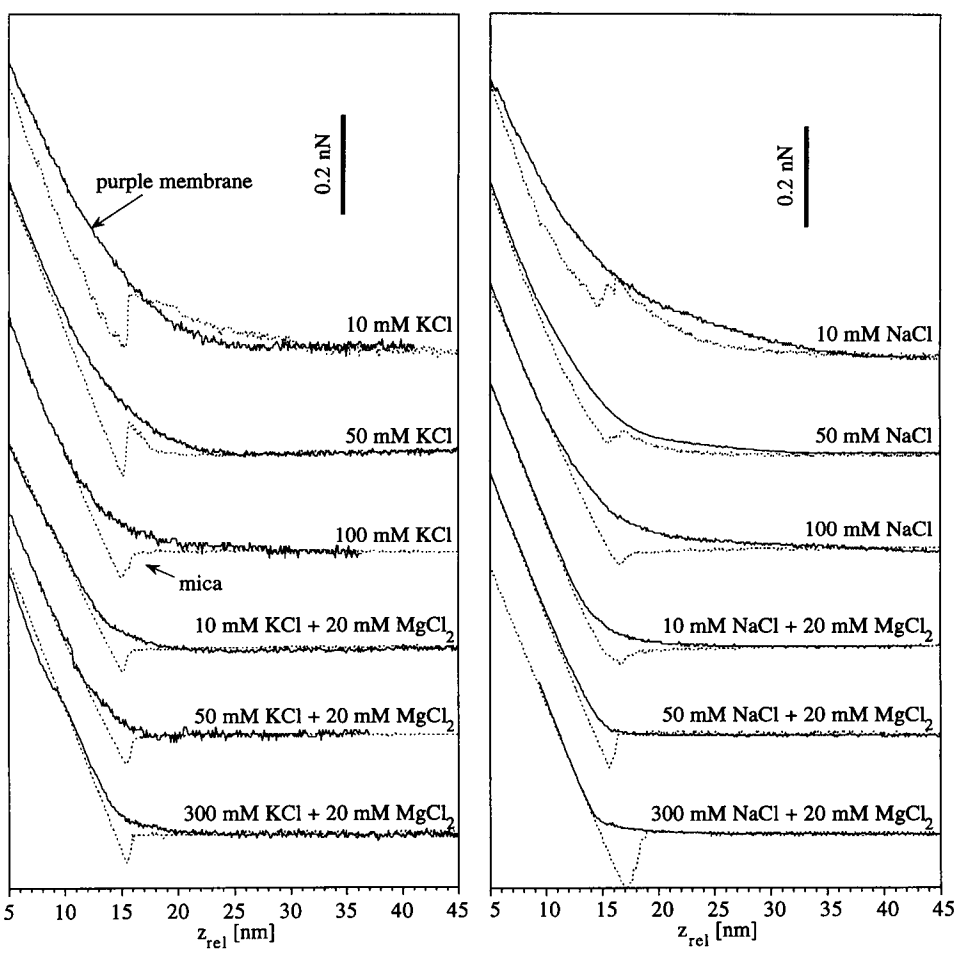

FIGURE 7 Force distance curves measured on mica (·····) and purple membrane (——), as a function of electrolyte concentration of the buffer solution (pH 8.2, 5–20 mM Tris-HCl). Conditions: scan frequency 2.4 Hz, scan range 50 nm (512 pixel). Each curve represents the average of 10 force curves.

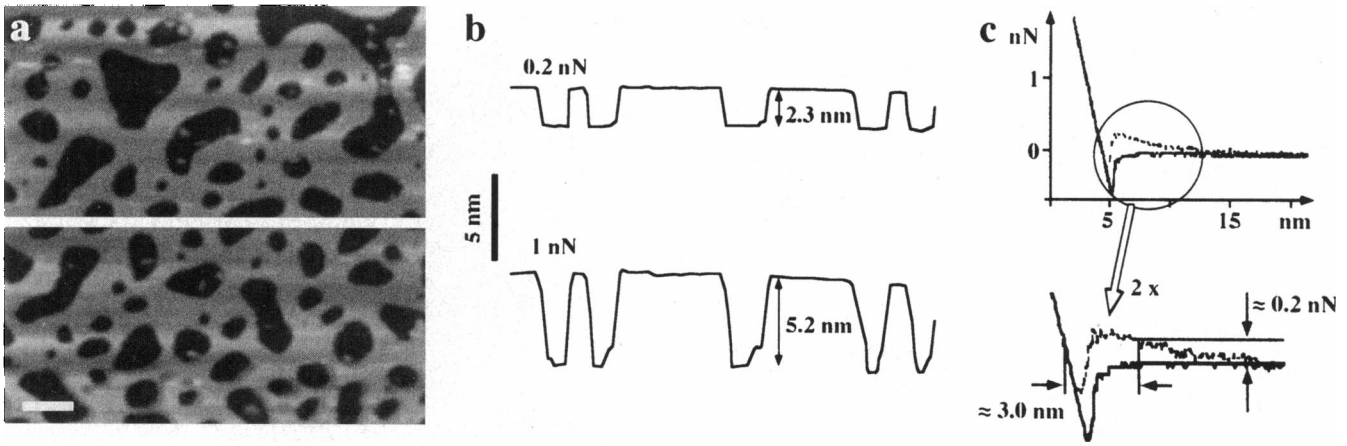

FIGURE 8 DPPE bilayer in electrolyte solution (pH 8.2, 5 mM KCl). (*a*) The height image shows bilayers adsorbed to mica. (*b*) Height plot along the line marked in *a*. The height between the bilayer and the mica surface was determined to be 5.3 ± 0.4 nm (n = 46) at a force of 1 nN, but was 2.3 ± 0.4 nm (n = 35) when the force was 0.2 nN. (*c*) Force curves were recorded on DPPE (——) and mica (·····) as the tip approached the sample. Each force curve is an average of 10 measurements; scan frequency 1.97 Hz, scan range 50 nm (512 pixels). The differences between DPPE and mica in the 0.1-nN range are clearly visible in the enlargement. Imaging conditions: ~0.6 nN, scan frequency 5.1 Hz. Scale bar 200 nm. The gray scale from dark to light shades represents 20 nm in *a*.

ious sizes. Phosphatidylethanolamine (PE) is a dominant phospholipid headgroup in biological membranes. It shows a dipole moment with its positive (amino group) charge closer to the AFM tip than the negative (phosphate) charge. The line indicated (Fig. 8 *a*) was used to determine the height between the bilayer and the mica. Imaged at forces of ~0.2 nN, the membrane showed a height of 2.3 ± 0.4 nm (Fig. 8 *b*, *top*). When imaged at forces of ~1 nN, however, the bilayer showed a height of 5.3 ± 0.4 nm (Fig. 8 *b*, *bottom*). Force curves were recorded on mica (Fig. 8 *c*, *dotted line*) and on the bilayer (Fig. 8 *c*, *solid line*) directly after the image was taken. As in purple membrane (Fig. 2), significant differences between both force curves were visible at forces below 0.3 nN. In this region the force curves on mica showed a repulsive interaction, whereas the tip snapped into an attractive interaction with the mica at higher force (cf. Fig. 7; Butt, 1991a,b). On the DPPE bilayer the interaction with the tip was attractive, even at such low electrolyte concentrations. Thus, if the sample was scanned at forces < 0.3 nN, the tip was not in contact with the mica, but with the bilayer. Therefore the measured height was smaller in this case than the structural thickness of the DPPE bilayer.

The thicknesses of reconstituted OmpF and AQP1 2D crystals, of HPI layers, and of DPPE were measured as function of the electrolyte concentration applying a force between 0.1 and 0.2 nN to the tip (Fig. 9). For unambiguous identification of the surface exposed to the tip and as a quality check, the topographs of the 2D crystals were always imaged at submolecular resolution before height measurements (Fig. 10). As in the purple membrane, the apparent heights of these regular protein arrays adsorbed to mica increased when the electrolyte concentration was smaller than a critical value. The measured heights of the periplasmic surface of OmpF crystals and of the AQP1 crystals showed the strongest dependence on the electrolytes. At a monovalent electrolyte concentration of ≥300 mM, they exhibited heights comparable to the structural thickness of the OmpF single layer (6.1 ± 0.2 nm; Schabert et al., 1995) and of the AQP1 layer (5.8 ± 0.4 nm; Walz et al., 1996). When the KCl concentration was decreased to 50 mM (pH 8.2), these heights increased by ~6 nm. HPI adsorbed to mica with its hydrophilic extracellular surface (Müller et al., 1996a). Consequently, the cytosolic surface was directed toward the tip. At an electrolyte concentration of 50 mM, the electrostatic contribution for the inner surface of HPI was 2 nm, and that for the extracellular surface of porin was 3 nm. In contrast to the protein layers, DPPE bilayers exhibited a negative electrostatic contribution, and their height decreased with decreasing electrolyte concentration.

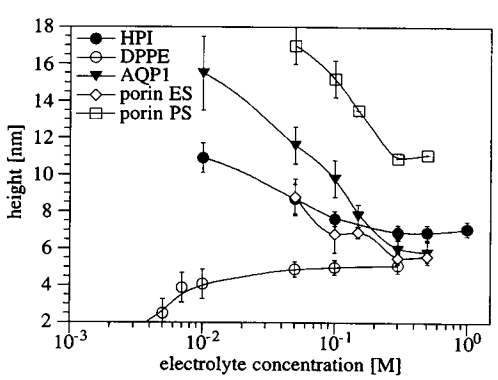

FIGURE 9 Height differences between biological systems and mica, as a function of monovalent electrolyte concentration. The electrolyte for HPI, DPPE, and OmpF was KCl, and that for AQP1 was NaCl. Porin ES and porin PS refer to measurements performed on the extracellular and the periplasmic surface, respectively. The periplasmic surface was only monitored on a double layer of OmpF sheets. In all measurements the pH was 8.2 (buffered by 1–20 mM Tris-HCl), and the force applied to the tip was 0.1 ± 0.05 nN.

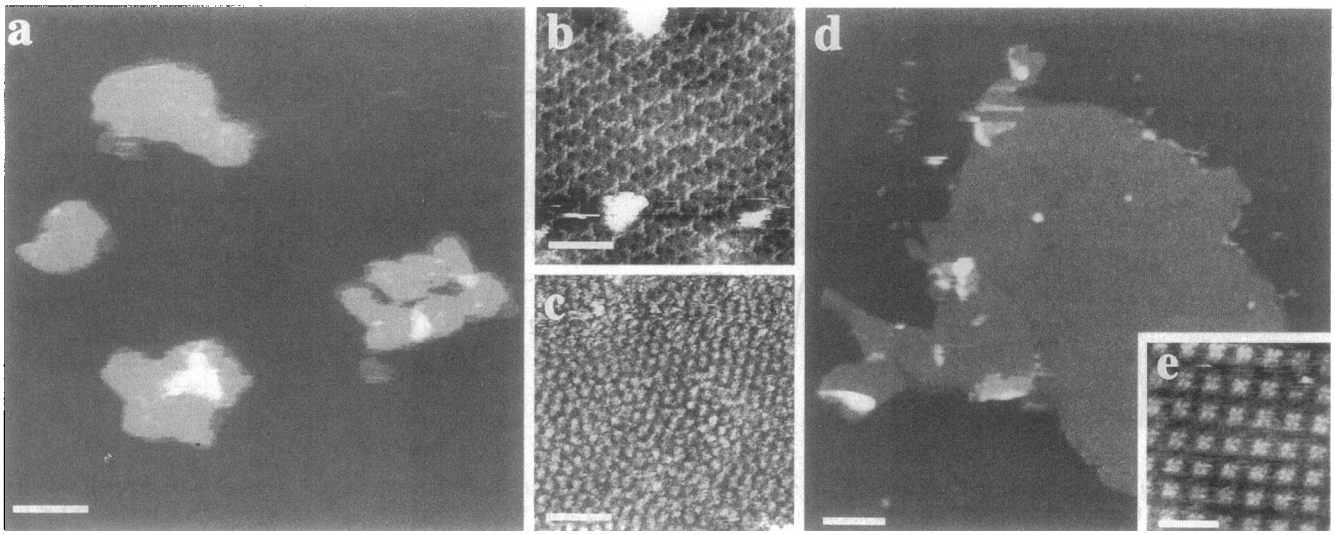

FIGURE 10 Surveys and high-resolution topographs of OmpF and AQP1 recorded in buffer solution. (*a*) Reconstituted OmpF sheets attached to mica. The sheets had diameters of up to 1 μm. (*b*) High-resolution image of the periplasmic surface, showing a rectangular lattice. (*c*) High-resolution image of the extracellular surface. Triplet protrusions belonging to a porin trimer are difficult to identify in the rectangular packing arrangement. (*d*) Crystalline AQP1 sheet adsorbed to mica. The sheets showed diameters of several microns. (*e*) High-resolution topograph of the AQP1 tetramers. Imaging conditions: 300 mM KCl, 20 Tris-HCl, pH 7.2 for OmpF; and 150 mM KCl, 10 Tris-HCl, pH 7.8 for AQP1. Gray level ranges, 20 nm in *a* and *d*, 4 nm in *c*, and 2 nm in *b* and *e*. Scale bars, 500 nm in *a* and *d*, and 20 nm in *b*, *c*, and *e*.

At 300 mM KCl, the DPPE height was ~5.3 nm, and it was 2.5 nm at 5 mM KCl.

pH dependence of the purple membrane height

As shown in Fig. 11 *a*, the height of purple membrane recorded at constant force (~0.2 nN) depended on the pH of the electrolyte solution. In basic solutions up to pH 10.5, the height measured at a particular electrolyte concentration was constant within the standard deviation. In contrast, the height of the membranes increased below pH 7 with decreasing pH, with a small drop toward pH 3. Although the general pH dependence of the measured height was found for all salt concentrations tested, the effect was less pronounced at high salt concentration. When imaged at applied forces of ~1 nN in 40 mM KCl, the height of the purple membrane remained constant (~5.6 ± 0.2 nm) above pH 6. Below pH 6 it decreased to a plateau of 5.2 ± 0.2 nm (pH 3.1). Force curves recorded on mica in 40 mM KCl at pH 8.4 (5 mM Tris-HCl; Fig. 11 *b*) showed a small repulsive interaction with the Si_3N_4 tip followed by an attractive interaction at closer distances. On purple membrane, the force curve was repulsive throughout. On both mica and purple membrane, the force curve characteristics changed when the pH was decreased. At pH 4.1 (Fig. 11 *b*), the repulsive interaction between the tip and mica vanished, whereas the repulsive interaction between the tip and the purple membrane increased slightly, thereby explaining the height anomaly observed at low pH.

Surface charge density determination

The surface charge density can be estimated from the height-versus-electrolyte concentration plots measured for AQP1, OmpF, HPI layer (Fig. 9), and purple membrane (Fig. 3). In these measurements, three regions may be differentiated (Fig. 12 *a*). At very low salt concentrations, the electrostatic repulsion of both mica and sample must be considered (region I; $z_1 \neq z_2 \neq 0$; see Fig. 4). At intermediate concentrations, the repulsion of mica is suppressed (region II; $z_1 = 0$; $z_2 \neq 0$). At high salt concentrations, the electrostatic repulsion of the protein sample is reduced as well, and the van der Waals attraction may not be neglected (region III; $z_1 = 0$; $z_2 \approx 0$). In regions I and II the force applied to the tip is equal to the electrostatic repulsion:

$$F_{\text{appl.}} = F_{\text{el}}(z) = \frac{4\pi\sigma_s\sigma_t R\lambda_D}{\epsilon_e\epsilon_0} e^{-z/\lambda_D} \tag{3}$$

If the tip is in contact with the support but not with the biological sample, as in the case of region II for the proteineous layers studied here, the difference between measured height h and structural height d corresponds to the electrostatic height contribution of the protein alone:

$$\Delta z(e_c) = -\frac{0.304}{\sqrt{e_c}} \ln\left(\frac{F_{\text{appl.}}\epsilon_e\epsilon_0\sqrt{e_c}}{4\pi R\sigma_s\sigma_t 0.304}\right) \tag{4}$$

Assuming a tip force of 0.1 nN, and considering the tip to have a surface charge density of -0.032 C/m^2 (Butt, 1991), the curves of Fig. 12 were fitted with Eq. 4 to the data points in region II to yield the surface charge densities. The known surface charge density of purple membrane (-0.05 C/m^2 (Butt, 1992)) was used to determine the tip radius (120 nm). The surface charge densities thus determined varied considerably: -0.0035 C/m^2 (inner surface of HPI), -0.01 C/m^2 (extracellular surface of OmpF), -0.06 C/m^2 (AQP1), and -0.08 C/m^2 (periplasmic surface of OmpF). The height

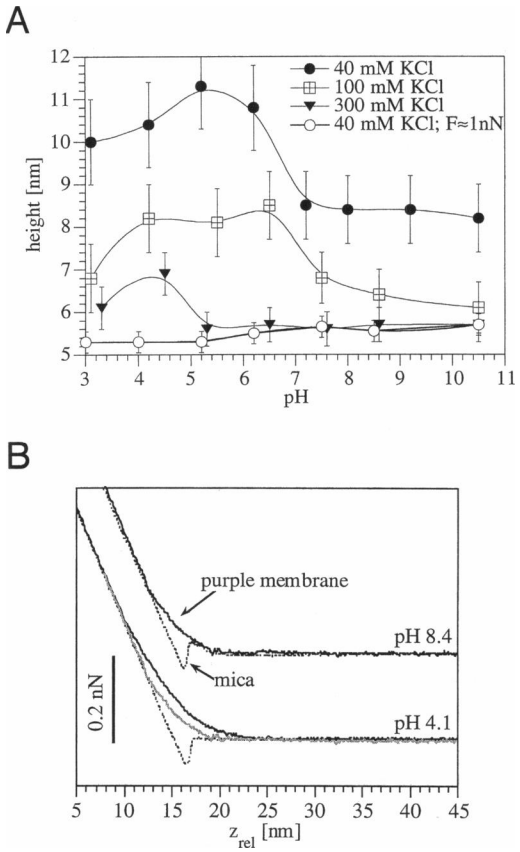

FIGURE 11 (*a*) Height of purple membrane adsorbed to mica versus pH of the buffer solution. Each point represents an average of more than 50 measurements on different membranes. The force applied was between 0.1 and 0.2 nN in all measurements, except for the sets recorded in 40 mM KCl and at 1 nN (○). The latter measurement shows the height change of bacteriorhodopsin at its pI from 5.6 nm to 5.2 nm (Müller et al., 1995b). (*b*) Force curves recorded at 40 mM KCl on purple membrane (*solid curves*) and on mica (*dotted curves*). The electrostatic repulsion on mica at pH 8.4 was larger than at pH 4.1. In contrast, the repulsion on purple membrane was larger at pH 4.1 (*upper curve in the lower graph*) than at pH 8.4 (*middle curve in the lower graph*). Conditions for recording the force curves: scan frequency 1.97 Hz, scan range 50 nm (512 pixels); each curve represents the average of 10 measurements. The buffers used were citric acid for pH 3–6, MES for pH 6–7, and Tris for pH 7–10. Their concentration was 5 mM in the presence of 40 mM KCl, and 10 mM with 100 mM KCl and above. The ion concentration (NaOH or HCl) added to adjust the pH of the buffer solution was between 0.6 and 7 mM (for 5 mM buffer) and 1 and 14 mM (for 10 mM buffer).

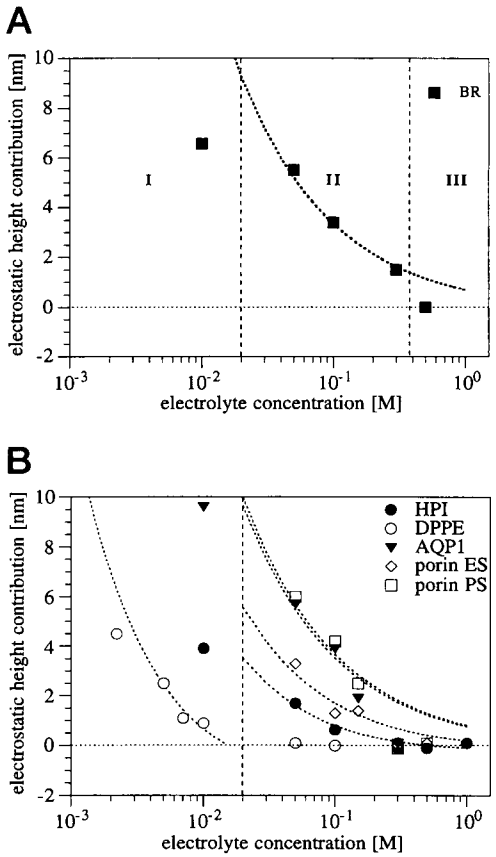

FIGURE 12 Simulation of the electrostatic contribution to the structural thickness of the biological samples. (*a*) Electrostatic contribution of bacteriorhodopsin. In region I, both bacteriorhodopsin and mica showed repulsive electrostatic contribution. In region II, mica no longer showed a repulsive contribution. In region III, van der Waals forces cannot be neglected, because the electrostatic repulsion is reduced. Therefore only the experimental data in region II were considered for fitting the curve given by Eq. 4. (*b*) Fits of the electrostatic contributions of AQP1, the inner surface of HPI, mica, and the extracellular (ES) and periplasmic (PS) surfaces of OmpF. Because the electrostatic repulsion of mica at monovalent electrolyte concentrations of <20 mM cannot be neglected, only experimental data above 20 mM (except for the values of DPPE) were taken into account for the fit. Experimental data points that indicated the elimination of electrostatic repulsion were neglected as well. Because DPPE showed virtually no repulsion of the AFM tip at low salt concentration, the electrostatic contribution of the mica surface was numerically simulated at concentrations of <20 mM.

anomalies of DPPE bilayers exhibited a different behavior, because they resulted from the electrostatic repulsion of mica (cf. Fig. 8). Therefore, DPPE heights at electrolyte concentrations of ≤10 mM simulated with Eq. 4 yielded a mica surface charge of -0.001 C/m^2.

DISCUSSION

The measurements and calculations presented here demonstrate that the height of a macromolecule recorded in an AFM image depends on the tip (Si_3N_4 in all measurements), the force applied, the aqueous environment, and the surface properties of both the sample and its support. This phenomenon is explained by the relative strength of electrostatic double-layer and van der Waals forces, and can be described by the DLVO theory (Butt et al., 1995). If the forces applied for contact mode imaging are smaller than the electrostatic double-layer repulsion, the measured height of a biological sample not only is of structural origin, but also shows an electrostatic contribution, and depends on the applied force. If the surface charge density of the sample exhibits the same polarity as tip (Si_3N_4) and support (mica) but is larger, the electrostatic contribution to the height measured with the AFM is positive. This was illustrated for AQP1, HPI, OmpF, and purple membrane, all of which have a net

negative surface charge at pH 8.2. If the surface charge density of the sample is less negative than that of mica, the electrostatic contribution is negative, as was demonstrated with DPPE bilayers. Sufficiently high forces (i.e., larger than the repulsive double layer force) must therefore be applied to ensure contact between the tip and the surfaces of both the biological object and its support. However, the structural flexibility of macromolecules (Müller et al., 1995a) and of cells (Radmacher et al., 1993, 1995; Hoh and Schoenenberger, 1994) must also be considered. If the applied forces are too large, an elastic deformation of the sample occurs (Weisenhorn et al., 1993), and the measured height no longer represents the thickness of the native sample.

Purple membranes exhibited a thickness of 5.5 ± 0.4 nm when imaged in a ≥300 mM monovalent salt solution at pH 8.2 for forces applied to the tip between 0.1 and 0.2 nN (Fig. 3), and 5.6 ± 0.2 nm at a salt concentration of ≥40 mM and a force of ~1 nN (Fig. 11). These values agree with results from x-ray scattering (Blaurock and Stoeckenius, 1971) and cryoelectron microscopy (Henderson, 1975; Henderson et al., 1990) (see Table 1). We could not detect a difference in the measured thickness between purple membranes that exposed their cytosolic surface and those that exposed their extracellular surface to the AFM tip. This suggests that both surfaces have charge densities that are equal within the error limits of our measurements (for a discussion of the surface charge density of purple membrane see Butt, 1992a).

To avoid damage due to friction, the applied force used to image purple membrane in the constant force mode may not be much larger than 1 nN. During force curve measurements, purple membranes were only disrupted when forces exceeded 2 nN. These thresholds are consistent with our previous observations that forces applied to the tip have to be below 1 nN to achieve submolecular resolution on biological samples (Karrasch et al., 1994; Schabert and Engel, 1994; Müller et al., 1995a, 1996a). However, parameters such as tip radius, buffer solution, and thermal drift all influence the conditions under which the membranes are disrupted by their interaction with the tip.

It is interesting to compare our previous measurements of purple membrane thickness variations as a function of pH with the current data shown in Fig. 11 *a*. Whereas a distinct decrease in the purple membrane thickness below the pI of bacteriorhodopsin (between 5.2 and 5.6; Ross et al., 1989) was observed at applied forces of 1 nN (cf. Fig. 11 *a*; Müller et al., 1995b), the height increased at acidic pH in various salt solutions when the membranes were scanned at forces of 0.2 nN (Fig. 11 *a*). The latter effect was unexpected. Changes in the ion concentration due to the pH adjustment of the buffer solution were small compared to the KCl concentration and could not account for the observed height variations (cf. Fig. 3). However, the pI of both a SiO_2 (≈ mica) surface and Si_3N_4 (tip) surface lies at pH 6 (Lin et al., 1993). Hence, as observed by force curve measurements (Fig. 11 *b*), the surface charges of the tip and the mica were neutralized around pH 6, thereby reducing the repulsive double-layer force. The change in surface charges also influences the interaction between the tip and the purple membrane. The force curves in Fig. 11 *b* demonstrate that the electrostatic interaction was repulsive. This might be expected, as pH 4.1 is lower than the pI of both tip and membrane. Thus the variation in the measured height is related to the change in the surface charge densities of the tip, mica, and purple membrane. Salt concentrations above 300 mM (KCl) were required to screen this electrostatic effect. Finally, when the force applied to the tip was 1 nN, the thickness decreased to 5.2 ± 0.2 nm below pH 6, corroborating our previous measurements (Fig. 11 *a*; Müller et al., 1995b).

For DPPE the bilayer spacing measured by x-ray diffraction is 6.0 nm, 5.7 nm, and 5.2 nm for the gel phase, crystalline phase, and fluid phase, respectively (Seddon et al., 1984). Thus the height of DPPE layers adsorbed to mica measured with the AFM (5.3 ± 0.4 nm) suggests that the bilayers created by the vesicle fusion method are either in the fluid or in the crystalline phase. This unexpected result may be explained by residual solvent trapped in the hydrocarbon core of the bilayer. Whereas DPPE exhibited an apparent decrease in thickness at low salt concentrations, the contrary was found with the lipid bilayer surrounding purple membrane patches. This was not unexpected, as the purple membrane contains glycolipids that are negatively charged at pH 8.2.

Because the electrostatic force shows an exponential dependence on distance, it is smaller than the van der Waals force, which has a reciprocal dependence when the tip is sufficiently close to the support or the sample surface. These different relationships imply different interaction areas of the two forces with the AFM tip. For a double-layer thickness that is larger than the tip radius, the entire tip interacts with the sample and the tip geometry cannot be neglected. In this case, the simple model of a sphere approaching a smooth surface (Eq. 2) does not describe the interaction properly, explaining discrepancies between the calculated and experimental forces. Indeed, the forces between the sample and individual tips can differ, even if the materials and electrolyte are identical. To overcome the problem of unknown tip geometry, micrometer-sized spheres have been attached to the AFM cantilever for the detection of force curves (Ducker et al., 1991). Equation 2 shows that a larger radius results in a higher force and thus allows force curves to be detected with a higher sensitivity. However, the lateral resolution of the AFM is reduced by increasing the tip radius.

The surface charge densities of various samples were determined from the dependence of the measured heights on the electrolyte concentration. The results rely on the accuracy of the measured purple membrane surface charge density (-0.05 ± 0.025 C/m^2; Butt, 1992b), which was chosen as a reference and used to calculate a tip radius of 120 nm. The fit of the curve given by Eq. 4 to the experimental data is shown in Fig. 12 *a*. It is evident that such a tip would not allow images exhibiting submolecular resolution to be ac-

quired (Figs. 2 and 10). However, all measurements were carried out with tips of excellent quality, and samples were systematically checked at high magnification before height measurements or force curve acquisition. In addition, scanning electron microscopy consistently revealed tip radii much smaller than 120 nm. We conclude that the pyramid-shaped tips used are equivalent to a sphere with a radius of 120 nm within the theoretical framework discussed here. The surface charge density of -0.001 C/m^2 determined for mica is 2.5 times smaller than that of -0.0025 C/m^2 measured by Pashley (1981). Nevertheless, both values lie within the experimental error (cf. Butt, 1992b), further supporting the consistency of the method.

CONCLUSIONS

To determine the true height of soft biological samples with the AFM, the electrolyte concentration and the pH of the buffer solution must be adjusted to screen the repulsive electrostatic interactions. The conditions can be determined by measuring heights as a function of electrolyte concentration at forces applied to the tip of ≤ 0.2 nN, and adjusting the concentration of the electrolyte to a point where possible electrostatic repulsion is eliminated. Such small forces are required to prevent significant elastic deformations of flexible biological molecules (Müller et al., 1995a). Heights measured by this procedure do not depend on characteristic surface charge densities, nor are they influenced by sample deformations.

The dependence of measured heights on the electrolyte concentration and pH opens the possibility of mapping surface charges of native biological macromolecules at subnanometer resolution. As surface charges govern the interaction of biomolecules, such data will provide new insight into fundamental biological processes at the molecular level.

We are grateful to Dr. S. Müller and Dr. B. Heymann for proofreading and discussing the manuscript, and M. Häner, D. Fotiadis, and S. Scheuring for fruitful discussions. We thank Dr. W. Baumeister for providing the HPI sample, Dr. G. Büldt for the purple membrane, Dr. A. Hoenger for the OmpF crystals, and Dr. T. Walz for the AQP1 crystals. DJM is grateful to Dr. G. Büldt for his continuous encouragement.

This work was supported by the Deutsche Forschungsgemeinschaft (SFB 189 to DJM), by the Swiss National Research Foundation (grant 4036-044062 to AE), and by the M. E. Müller Foundation.

REFERENCES

Apell, H.-J., J. Colchero, A. Linder and O. Marti. 1993. Investigation of Na, K-ATPase by SFM. *In* STM and AFM in Biology. O. Marti and M. Amrein, editors. Academic Press, London. 275–308.

Bailey, S. W. 1984. Classification and structures of the micas. *In* Micas. S. W. Bailey, editor. Mineralogical Society of America. 1–92.

Baumeister, W., F. Karrenberg, R. Rachel, A. Engel, B. Ten Heggeler, and W. O. Saxton. 1982. The major cell envelope protein of *Micrococcus radiodurans* (R1). *Eur. J. Biochem.* 125:535–544.

Binnig, G., C. F. Quate, and C. Gerber. 1986. Atomic force microscope. *Phys. Rev. Lett.* 56:930–933.

Blaurock, A. E., and W. Stoeckenius. 1971. Structure of the purple membrane. *Nature New Biol.* 233:152–154.

Bremer, A., Ch. Henn, A. Engel, W. Baumeister, and U. Aebi. 1992. Has negative stain still a place in biomacromolecular electron microscopy? *Ultramicroscopy.* 46:85–111.

Butt, H.-J. 1991a. Electrostatic interaction in atomic force microscopy. *Biophys. J.* 60:777–785.

Butt, H.-J. 1991b. Measuring electrostatic, van der Waals, and hydration forces in electrolyte solutions with an atomic force microscope. *Biophys. J.* 60:1438–1444.

Butt, H.-J. 1992a. Electrostatic interaction in scanning probe microscopy when imaging in electrolyte solutions. *Nanotechnology.* 3:60–68.

Butt, H.-J. 1992b. Measuring local surface charge densities in electrolyte solutions with a scanning force microscope. *Biophys. J.* 63:578–582.

Butt, H.-J., K. H. Downing, and P. K. Hansma. 1990. Imaging the membrane protein bacteriorhodopsin with the atomic force microscope. *Biophys. J.* 58:1473–1480.

Butt, H.-J., M. Jaschke, and W. Ducker. 1995. Measuring surface forces in aqueous solution with the atomic force microscope. *Bioelectrochem. Bioenerg.* 38:191–201.

Butt, H.-J., C. B. Prater, and P. K. Hansma. 1991. Imaging purple membranes dry and in water with the atomic force microscope. *J. Vac. Sci. Technol.* B9: 1193–1197.

Butt, H.-J., P. Siedle, K. Seifert, K. Fendler, T. Seeger, E. Bamberg, A. L. Weisenhorn, K. Goldie, and A. Engel. 1993. Scan speed limit in atomic force microscopy. *J. Microsc.* 169:75–84.

Drake, B., C. B. Prater, A. L. Weisenhorn, S. A. C. Gould, T. R. Albrecht, C. F. Quate, D. S. Cannell, H. G. Hansma, and P. K. Hansma. 1989. Imaging crystals, polymers, and processes in water with the atomic force microscope. *Science.* 243:1586–1588.

Ducker, W. A., T. J. Senden, and R. M. Pashley. 1991. Direct measurements of colloidal forces using an atomic force microscope. *Nature.* 353:239–241.

Fritz, M., M. Radmacher, M. W. Allersma, J. P. Cleveland, R. J. Stewart, P. K. Hansma, and C. F. Schmidt. 1995a. Imaging microtubles in buffer solution using tapping mode atomic force microscopy. *SPIE.* 2384: 150–157.

Fritz, M., M. Radmacher, J. P. Cleveland, M. W. Allersma, R. J. Steward, R. Gieselmann, P. Janmey, C. F. Schmidt, and P. K. Hansma. 1995b. Imaging globular and filamentous proteins in physiological buffer solutions with tapping mode atomic force microscopy. *Langmuir.* 11: 3529–3535.

Hansma, H. G., D. E. Laney, M. Bezanilla, R. L. Sinsheimer, and P. K. Hansma. 1995. Applications for atomic force microscopy of DNA. *Biophys. J.* 68:1672–1677.

Henderson, R. 1975. The structure of the purple membrane from *Halobacterium halobium*: analysis of the x-ray diffraction pattern. *J. Mol. Biol.* 93:123–138.

Henderson, R., J. M. Baldwin, T. A. Ceska, F. Zemlin, E. Beckman, and K. H. Downing. 1990. Model for the structure of bacteriorhodopsin based on high-resolution electron cryo-microscopy. *J. Mol. Biol.* 213: 899–929.

Hoenger, A., R. Ghosh, C.-A. Schoenenberger, U. Aebi, and A. Engel. 1993. Direct in situ structural analysis of recombinant outer membrane proteins expressed in an OmpA-deficient mutant *Escherichia coli* strain. *J. Struct. Biol.* 111:212–221.

Hoh, J. H., R. Lal, S. A. John, J.-P. Revel, and M. F. Arnsdorf. 1991. Atomic force microscopy and dissection of gap junctions. *Science.* 253:1405–1408.

Hoh, J. H., and C.-A. Schoenenberger. 1994. Surface morphology and mechanical properties of MDCK monolayers by atomic force microscopy. *J. Cell Sci.* 107:1105–1114.

Hoh, J. H., G. E. Sosinsky, J.-P. Revel, and P. K. Hansma. 1993. Structure of the extracellular surface of the gap junction by atomic force microscopy. *Biophys. J.* 65:149–163.

Israelachvili, J. 1991. Intermolecular and Surface Forces, 2nd Ed. Academic Press, London.

Israelachvili, J. 1994. Molecular adhesion and tribiology. Troisieme cycle de la physique en suisse romande, Universités de Berne, Fribourg, Genève, Lausanne, EPF de Lausanne et Neuchâtel.

Jap, B. K., M. Zulauf, T. Scheybani, A. Hefti, W. Baumeister, U. Aebi, and A. Engel. 1992. 2D crystallization: from art to science. *Ultramicroscopy.* 46:45–84.

Jungblut, H., S. A. Campbell, M. Giersig, D. J. Müller, and H. J. Lewerenz. 1992. Scanning tunneling microscopy observations of biomolecules on layered materials. *Faraday Discuss.* 94:183–198.

Karrasch, S., M. Dolder, J. Hoh, F. Schabert, J. Ramsden, and A. Engel. 1993. Covalent binding of biological samples to solid supports for scanning probe microscopy in buffer solution. *Biophys. J.* 65: 2437–2446.

Karrasch, S., R. Hegerl, J. Hoh, W. Baumeister, and A. Engel. 1994. Atomic force microscopy produces faithful high-resolution images of protein surfaces in an aqueous environment. *Proc. Natl. Acad. Sci. USA.* 91:836–838.

Lin, X.-Y., F. Creuzet, and H. Arribart. 1993. Atomic force microscopy for local characterization of surface acid-base properties. *J. Phys. Chem.* 97:7272–7276.

Mou, J. X., D. M. Czajkowsky, Y. Y. Zhang, and Z. F. Shao. 1995a. High-resolution atomic-force microscopy of DNA: the pitch of the double helix. *FEBS Lett.* 371:279–282.

Mou, J., S. Sheng, R. Ho, and Z. Shao. 1996. Chaperonins GroEL and GroES: views from atomic force microscopy. *Biophys. J.* 71:2213–2221.

Mou, J. X., J. Yang, and Z. F. Shao. 1994. Tris(hydroxymethyl)aminomethane ($C_4H_{11}NO_3$) induced a ripple phase in supported unilamellar phospholipid bilayers. *Biochemistry.* 33:4439–4443.

Mou, J. X., J. Yang, and Z. F. Shao. 1995b. Atomic force microscopy of cholera toxin B-oligomers bound to bilayers of biologically relevant lipids. *J. Mol. Biol.* 248:507–512.

Müller, D. J., W. Baumeister, and A. Engel. 1996a. Conformational change of the hexagonally packed intermediate layer imaged by atomic force microscopy. *J. Bacteriol.* 178:3025–3030.

Müller, D. J., G. Büldt, and A. Engel. 1995a. Force-induced conformational change of bacteriorhodopsin. *J. Mol. Biol.* 249:239–243.

Müller, D. J., M. Amrein, and A. Engel. 1997a. Adsorption of biological molecules to a solid support for scanning probe microscopy. *J. Struct. Biol.* (in press).

Müller, D. J., A. Engel, and M. Amrein. 1997b. Preparation techniques for the observation of native biological systems with the atomic force microscope. *Biosens. Bioelectron.* (in press).

Müller, D. J., A. Engel, J. Carrascosa, and M. Veléz. 1997c. The bacteriophage ø29 head-tail connector imaged at high resolution with atomic force microscopy in buffer solution. *EMBO J.* 16:103–107.

Müller, D. J., F. A. Schabert, G. Büldt, and A. Engel. 1995b. Imaging purple membranes in aqueous solutions at subnanometer resolution by atomic force microscopy. *Biophys. J.* 68:1681–1686.

Müller, D. J., C. A. Schoenenberger, G. Büldt, and A. Engel. 1996b. Immuno-atomic force microscopy of purple membrane. *Biophys J.* 70: 1796–1802.

Oesterhelt, D., and W. Stoeckenius. 1974. Isolation of the cell membrane of *Halobacterium halobium* and its fraction into red and purple Membrane. *Methods Enzymol.* 31:667–678.

Ohnesorge, F., and G. Binnig. 1993. True atomic resolution by atomic force microscopy through repulsive and attractive forces. *Science.* 260: 1451–1456.

Pashley, R. M. 1981. Hydration forces between mica surfaces in Li^+, Na^+, Na^+ and Cs^+ electrolyte solutions: a correlation of double layer and hydration forces with surface cation exchange properties. *J. Colloid Interface Sci.* 83:531–546.

Rädler, J., M. Radmacher, and H. E. Gaub. 1994. Velocity-dependent forces in atomic force microscopy imaging of lipid films. *Langmuir.* 10:3111–3115.

Radmacher, M., M. Fritz, and P. K. Hansma. 1995. Imaging soft samples with the atomic force microscope: gelatin in water and propanol. *Biophys. J.* 69:264–270.

Radmacher, M., R. W. Tillman, and H. E. Gaub. 1993. Imaging viscoelsaticity by force modulation with the atomic force microscope. *Biophys. J.* 64:735–742.

Ross, P. E., S. L. Helgerson, L. J. W. Miercke, and E. A. Dratz. 1989. Isoelectric focusing studies of bacteriorhodopsin. *Biochim. Biophys. Acta.* 991:134–140.

Schabert, F. A., and A. Engel. 1994. Reproducible acquisition of *Escherichia coli* porin surface topographs by atomic force microscopy. *Biophys. J.* 67:2394–2403.

Schabert, F. A., C. Henn, and A. Engel. 1995. Native *Escherichia coli* OmpF porin surfaces probed by atomic force microscopy. *Science.* 268:92–94.

Schabert, F. A., and J. P. Rabe. 1996. Vertical dimension of hydrated biological samples in tapping mode scanning force microscopy. *Biophys. J.* 70:1514–1520.

Seddon, J. M., G. Cevc, R. D. Kaye, and D. Marsh. 1984. X-ray diffraction study of the polymorphism of hydrated diacyl- and dialkylphospatidylethanolamines. *Biochemistry.* 23:2634–2644.

Sugawara, Y., M. Ohta, H. Ueyama, and S. Morita. 1995. Defect motion on an InP(110) surface observed with noncontact atomic force microscopy. *Science.* 270:1646–1648.

Tatulian, S. A. 1993. Ionization and ion binding. *In* Phospholipids Handbook. G. Cevc, editor. Marcel Dekker, New York. 511–549.

Vikholm, I., J. Peltonen, and O. Teleman. 1995. Atomic force microscope images of lipid layers spread from vesicle suspensions. *Biomembranes.* 1233:111–117.

Walz, T., B. L. Smith, P. Agre, and A. Engel. 1994. The three-dimensional structure of human erythrocyte aquaporin chip. *EMBO J.* 13:2985–2993.

Walz, T., P. Tittmann, K. H. Fuchs, D. J. Müller, B. L. Smith, P. Agre, H. Gross, and A. Engel. 1996. Surface topographies at subnanometer-resolution reveal asymetry and sidedness of aquaporin-1. *J. Mol. Biol.* 264:907–918.

Weisenhorn, A. L., M. Khorsandi, S. Kasas, V. Gotzos, and H.-J. Butt. 1993. Deformation and height anomaly of soft surfaces studied with an AFM. *Nanotechnology.* 4:106–113.

Weisenhorn, A. L., P. Maivald, H.-J. Butt, and P. K. Hansma. 1992. Measuring adhesion, attraction and repulsion between surfaces in liquids with an atomic force microscope. *Phys. Rev. B.* 45:11226–11232.

Wilson, J. A., and A. D. Yoffe. 1969. The transition metal dichalcogenides: discussion and interpretation of the observed optical, electrical and structural properties. *Adv. Phys.* 18:193–335.

Wyman, C., E. Grotkopp, C. Bustamante, and H. C. M. Nelson. 1995. Determination of heat-shock transcription factor 2 stoichiometry at looped DNA complexes using scanning force microscopy. *EMBO J.* 14:117–123.

Yang, J., J. X. Mou, and Z. F. Shao. 1994. Structure and stability of pertussis toxin studied by in situ atomic force microscopy. *FEBS Lett.* 338:89–92.

Yang, J., L. K. Tamm, T. W. Tillack, and Z. Shao. 1993. New approach for atomic force microscopy of membrane proteins. *J. Mol. Biol.* 229: 286–290.